Journal of Biomedical Optics

SPIEDigitalLibrary.org/jbo

Spectroscopic photoacoustic imaging of lipid-rich plaques in the human aorta in the 740 to 1400 nm wavelength range

Thomas J. Allen
Andrew Hall
Amar P. Dhillon
James S. Owen
Paul C. Beard

SPIE

Spectroscopic photoacoustic imaging of lipid-rich plaques in the human aorta in the 740 to 1400 nm wavelength range

Thomas J. Allen,[a] Andrew Hall,[b] Amar P. Dhillon,[b] James S. Owen,[c] and Paul C. Beard[a]
[a]University College London, Department of Medical Physics and Bioengineering, Gower Street, WC1E 6BT London, United Kingdom
[b]Royal Free Campus, UCL Medical School, Department of Cellular Pathology, Rowland Hill Street, NW3 2PF London, United Kingdom
[c]Royal Free Campus, UCL Medical School, Division of Medicine, Rowland Hill Street, NW3 2PF London, United Kingdom

Abstract. Spectroscopic photoacoustic imaging has the potential to discriminate between normal and lipid-rich atheromatous areas of arterial tissue by exploiting the differences in the absorption spectra of lipids and normal arterial tissue in the 740 to 1400 nm wavelength range. Identification of regions of high lipid concentration would be useful to identify plaques that are likely to rupture (vulnerable plaques). To demonstrate the feasibility of visualizing lipid-rich plaques, samples of human aortas were imaged in forward mode, at wavelengths of 970 and 1210 nm. It was shown that the structure of the arterial wall and the boundaries of lipid-rich plaques obtained from the photoacoustic images were in good agreement with histology. The presence of lipids was also confirmed by comparing the photoacoustic spectra (740 to 1400 nm) obtained in a region within the plaque to the spectral signature of lipids. Furthermore, a lipid-rich plaque was successfully imaged while illuminating the sample through 2.8 mm of blood demonstrating the possibility of implementing the photoacoustic technique *in vivo*. [DOI: 10.1117/1.JBO.17.6.061209]

Keywords: photoacoustic imaging; photoacoustic spectroscopy; vulnerable plaques; lipid-rich plaques; atherosclerosis; intravascular imaging.

Paper 11527SSP received Sep. 20, 2011; revised manuscript received Nov. 18, 2011; accepted for publication Jan. 12, 2012; published online May 7, 2012.

1 Introduction

Atherosclerosis is a chronic disease characterized by the progressive buildup of plaque that begins in the inner lining of the arterial wall (intima).[1,2] Most infarctions are instigated by the rupturing of one or more atherosclerotic plaques, leading to the formation of a partial or complete occlusive thrombus. Plaques that exhibit a greater propensity to rupture are termed vulnerable plaques and are usually characterized by a thin fibrous cap overlaying a soft lipid pool and an increased abundance of macrophages.[3,4] In order to identify these plaques unambiguously prior to rupture, knowledge of their composition, as well as morphology, would be beneficial. Angiography is widely used to determine the location of a stenosis due to plaque buildup but does not provide structural or compositional information. Intravascular ultrasound (IVUS)[5] can image directly the full thickness of the arterial wall with high spatial resolution (<100 μm). Although it can reveal plaque morphology and identify the presence of calcification, it provides limited information relating to other constituents of atherosclerotic plaques, such as lipids. Intravascular optical coherence tomography (OCT)[6–8] can visualize plaque in coronary arteries with high spatial resolution (<10 μm). However, the penetration depth is limited to approximately 1 mm due to optical scattering, so it is unable to create images through the thickest plaques. The ability of OCT to discriminate unambiguously between lipid pools and calcifications can also be limited as both provide similar contrast (low backscattering), resulting in the sharpness of boundaries being the principal means to distinguish between the two tissue types.[7,9,10] It also requires the additional step of flushing the lumen of the vessel with saline to remove the blood prior to image acquisition. Other intravascular imaging modalities include angioscopy, thermography, Raman spectroscopy, and near-infrared (NIR) spectroscopy.[9,11,12] These can provide information relating to the superficial composition of the plaque, but not detailed depth resolved structural information. Non-invasive imaging methods include magnetic resonance imaging (MRI) and ultra-fast computed tomography (UFCT).[11–13] MRI can provide information regarding the composition of the plaque, but it generally suffers from motion artifacts when imaging the coronary artery, and it requires long acquisition times to obtain high-resolution images (<400 μm).[14,15] UFCT imaging methods provide adequate resolution, and acquisition times are sufficiently short to minimize motion artifacts but are limited to the detection of calcium deposits and require ionizing radiation.

Photoacoustic imaging can provide both structural and composition-related information based on optical absorption and thus offers the prospect of overcoming the limitations of other methods[16] for detecting vulnerable plaques. The technique involves illuminating the target tissue with nanosecond (ns) pulses of laser light. Absorption of the light creates a small localized temperature increase followed by an initial pressure rise that subsequently relaxes, resulting in the emission of broadband ultrasound waves. The detected photoacoustic signal provides a measure of the spatial distribution of the absorbed

Address all correspondence to: Thomas J. Allen, University College London, Department of Medical Physics and Bioengineering, Gower Street, WC1E 6BT London, United Kingdom. Tel.: +44 2076790291; E-mail: tjallen@medphys.ucl.ac.uk

0091-3286/2012/$25.00 © 2012 SPIE

optical energy, which is dependent principally upon the optical absorption properties of the tissue. By varying the wavelength of the laser source, spatially resolved spectroscopic information can therefore be obtained. The fundamental advantage of photoacoustic imaging is that, by encoding optical contrast on to acoustic waves, it avoids the limited penetration depth of purely optical imaging techniques such as OCT since acoustic waves are scattered much less than light. At the same time, the spectroscopic nature of the technique allows it to provide significantly higher contrast and specificity than conventional ultrasound imaging. An early study showed that atheroma could be identified using photoacoustic methods by exploiting the strong preferential absorption that lipid-rich plaques exhibit in the wavelength range 420 to 530 nm[17]—the source of contrast being the presence of carotenoids, which are related to the process of lipid accumulation. However, as well as being a somewhat indirect route to lipid detection, the use of these excitation wavelengths results in limited penetration depth in vascular tissue. They are also strongly absorbed by hemoglobin in blood. This would necessitate the use of a saline flush to deliver sufficient light to the vessel wall if implemented *in vivo* using an intravascular probe in a manner analogous to IVUS or OCT. Structural photoacoustic images of *ex vivo* vascular tissues have been obtained at 532 nm, although it offers no discernible discriminatory ability in terms of composition.[17] The 680 to 900 nm spectral range has also been explored,[18] the rationale being that features in the absorption spectrum of lipids within this wavelength range can be employed for discriminatory purposes. However, these spectral features are rather indistinct, so the discrimination is relatively weak. In addition, although optical absorption by blood is lower than that in the visible wavelength range, it is still sufficiently high to require the use of a saline flush.

Following these early studies, attention turned to the more promising longer near infrared (NIR) wavelength range 740 to 1400 nm, inspired by NIR spectroscopic studies of vascular tissue.[19–22] There are several factors that suggest this spectral range may be optimal for imaging lipid-rich plaques. First, the lipid absorption spectrum is well differentiated from the spectra of other constituents of vascular tissue, such as water, elastin, and collagen. This is particularly so at 1210 nm, where there is a large absorption peak. Second, although lipids exhibit relatively strong absorption in this wavelength range, it is not so high as to limit penetration depth excessively, thus offering the prospect of imaging through the full wall thickness of even a severely stenosed vessel. Third, in this spectral range, absorption by blood is low and dominated by water rather than hemoglobin and thus may obviate the need for a saline flush in an intravascular implementation. The prospect of exploiting the 740 to 1400 nm wavelength range for photoacoustic imaging of atherosclerosis was first reported by Allen and Beard in preliminary studies[23,24] and has since been explored in *ex vivo* studies of rabbit aorta,[25,26] porcine coronary arteries,[27] and fresh human coronary arteries.[28] The purpose of the study reported in this paper is twofold. The first goal is to corroborate these preliminary findings by undertaking a study using a dedicated laboratory bench-top tissue characterization setup. The second is to obtain an indication of the imaging performance and discrimination that might ultimately be achieved using an optimized detector, a rigorous approach to image reconstruction and processing and appropriate spectral analysis. To this end, spectroscopic photoacoustic images in the range 740 to 1400 nm that reveal the full thickness of postmortem human aortic samples and unambiguously visualize the shape and location of lipid pools in atheromatous plaques in accordance with histology were obtained. A further objective was to test the hypothesis that it is possible to obtain images of lipid-rich plaques through several millimeters of blood.

The spectral properties of the constituents of arterial tissues as a basis for discrimination are discussed in Sec. 2, the experimental imaging system used is described in Sec. 3, and the results of the tissue characterization studies undertaken are presented in Sec. 4.

2 Optical Properties of Arterial Tissue

The central hypothesis of this work is that the absorption spectra of lipids are sufficiently well differentiated from those of the constituents of normal arterial tissue in the 740 to 1400 nm wavelength range to permit the detection of lipid-rich plaques using spectroscopic photoacoustic imaging. This hypothesis is supported by several studies in which the optical absorption spectra of arterial tissue and lipids in the visible,[29–32] and NIR[33–35] wavelength range were measured. In the 740 to 1400 nm wavelength range, these studies have reported absorption peaks around 970 and 1180 nm in normal arterial tissue. These peaks correspond to the vibrational overtone of the O–H bonds of the water molecules (see Fig. 1), which compose 70% of normal arterial tissue.[36] The other principal chromophores present in normal arterial tissue are collagen and elastin. Their spectral signatures, also shown in Fig. 1, are relatively flat in the 900 to 1100 nm wavelength range with an absorption peak around 1180 nm. Collagen and elastin together make up less than 25% of normal arterial tissue, and therefore their contribution to the absorption spectrum of normal arterial tissue is significantly less than that of water. Lipids present in atherosclerotic lesions are mostly composed of cholesteryl ester (48%), phospholipids (26%), cholesterol (20%), and, to a lesser extent, triglyceride (6%).[37] The absorption spectra of these different lipids are relatively similar and characterized by three absorption peaks around 920, 1040, and 1210 nm, which correspond to overtones of the stretching vibration mode of the C-H bonds.[19] These spectral features, especially the large absorption peak at 1210 nm, suggest this wavelength range can be exploited to detect lipid rich plaques. In addition, absorption by blood beyond 1100 nm is dominated by water absorption

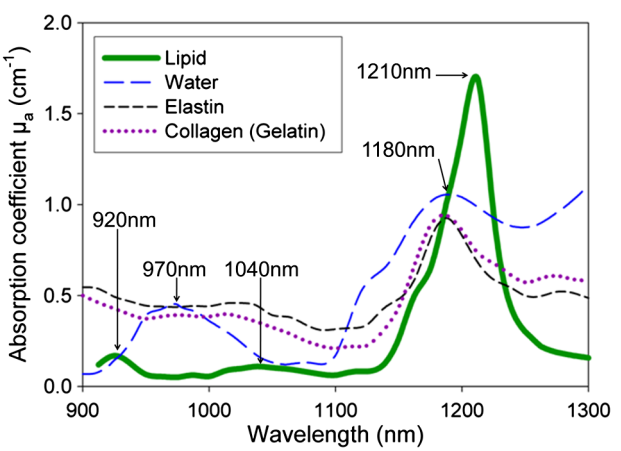

Fig. 1 Absorption coefficient spectra of lipid, water, elastin, and collagen.[35]

and is therefore relatively low. For example, at an excitation wavelength of 1210 nm, the penetration depth in blood, defined as the depth at which the irradiance has decreased by $1/e$, is approximately 1.14 mm, whereas at an excitation wavelength of 600 nm, the penetration is approximately 0.28 mm.[38,39] This suggests that it may be possible to image the arterial wall through blood without the need for a saline flush.

3 Experimental Method

3.1 *Experimental Setup*

In this study, the acoustic resolution photoacoustic microscopy (AR-PAM) mode of photoacoustic imaging was used.[16,40] This employs a focused ultrasound receiver and mechanical scanning to map the photoacoustic signals over the tissue surface. A schematic of the experimental setup used to generate and detect photoacoustic signals in arterial tissue is shown in Fig. 2. A fiber-coupled tuneable optical parametric oscillator (OPO)–based laser system was used to generate ns pulses in the 740 to 1400 nm wavelength range. The fluence was approximately 60 mJ/cm^2 when operating at an excitation wavelength of 970 nm and 40 mJ/cm^2 when operating at an excitation wavelength of 1210 nm. The excitation pulses were delivered via a glass window to the intimal side of the tissue sample, which was immersed in a saline bath. The beam incident on the tissue surface was approximately 5 mm in diameter. A spherically focused broadband polyvinylidene fluoride (PVDF) ultrasound detector (25 MHz), with a focal spot diameter of approximately 240 μm and a focal length of approximately 24 mm, was used to detect the generated photoacoustic signals in transmission mode. To obtain 2-D images, the tissue sample was mounted on a computer-controlled translation stage and mechanically scanned along a line in the x direction in steps of 500 μm. For each scan step, the detected photoacoustic signal was amplified (40 dB), signal-averaged 20 times, and then downloaded to a personal computer (PC). The axial resolution (limited by the transducer bandwidth) was 75 μm. The lateral resolution is limited ultimately by the 240 μm spot size of the transducer, although in this study, it was defined by the 500 μm scan step size used to acquire the images. Photoacoustic spectra were also obtained at a number of different points along the scan line, in the 740 to 1400 nm wavelength range and increments of 20 nm. The spectra were corrected for the wavelength-dependent pulse energy of the laser system and normalized to the amplitude of the measurements obtained at 960 nm. The spectra were plotted using a spline curve interpolation method.

To investigate the possibility of generating and detecting photoacoustic signals when illuminating the tissue sample through several millimeters of human blood to mimic intravascular conditions, the experimental setup was modified. The saline bath was partitioned in two sections: one containing saline and the other containing outdated human blood obtained from a blood bank (see Fig. 3). The partition was an acoustically transparent wall made from a 5 μm thick polyvinyl chloride (PVC) film. Blood that had exceeded the expiry date of thirty days since donation was obtained from the local hospital and diluted with phosphate-buffered saline, providing a hematocrit concentration of at least 30%. The red blood cells were kept constantly circulating, using a pump, to keep them from settling at the bottom of the cuvette.

3.2 *Image Reconstruction and Processing*

The detected photoacoustic signals were low-passed filtered (25 MHz), mapped to distance using the acoustic speed of sound in normal arterial tissue (1,575 m/s[41]), and any dc-offset removed. The signals were then integrated to obtain a depth profile of the absorbed optical energy density. Each depth profile or A-line was corrected for the exponential decay of the light distribution through tissue in a manner analogous to time-gain compensation in ultrasound imaging. The correction was achieved by dividing the A-lines by an exponential function, whose decay constant was selected to match that of the A-line in a region identified as normal tissue (near the rear boundary of the arterial wall). For the measurements obtained when immersing the tissue sample in blood, it was necessary to modify the method used to correct for the light attenuation, due to the strong background photoacoustic signal generated in blood. For these measurements, the rate of decay of the exponential function was selected to match that of the A-line in an area identified as containing blood. Correcting for the light distribution in this way prevented the background signal from dominating the photoacoustic image allowing for the structure of the arterial wall to be revealed. A 2-D image was then formed from the corrected A-lines by converting the amplitude of the signal to a grayscale and the low end of the scale bar was set to zero to threshold negative image intensity values. To reduce the image pixilation caused by the relatively large scanning steps (500 μm), the number of A-lines was also increased

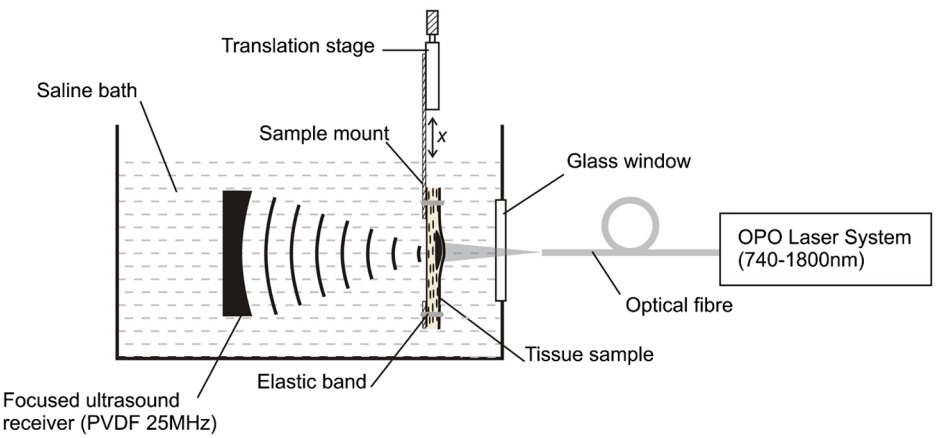

Fig. 2 Schematic of the experimental setup. The tissue sample was scanned by translating it along the x direction.

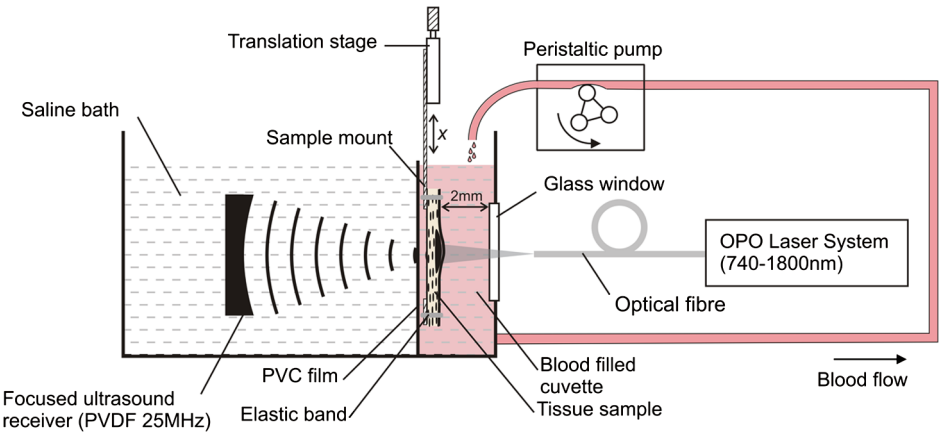

Fig. 3 Schematic of the experimental setup used when illuminating the sample through blood. The tissue sample was scanned by translating it along the *x* direction.

by interpolation. The interpolation was performed using a low-pass filtering method provided by the "interp" function within Matlab.

3.3 *Tissue Preparation*

The tissue samples were sections of human aortas fixed in formalin and suspended in ethanol and were obtained from the UK Human Tissue Bank (UKHTB). The start and finish points of the scan were marked on the tissue samples so that they could be registered with histological sections. After the experiments, the tissue samples were embedded in a paraffin wax matrix, sectioned at 4 μm and stained using hematoxylin and eosin (H&E).

4 Results

4.1 *Normal Arterial Tissue*

A section of human aorta identified by visual inspection as normal was opened out flat [Fig. 4(a)] and scanned over a distance of 10 mm in steps of 500 μm. Figure 4(b) and 4(c) shows 2-D photoacoustic images obtained at excitation wavelengths of 970 and 1210 nm, respectively. The excitation light was delivered to the intimal surface of the tissue [the top surface in Fig. 4(b) and 4(c)]. Both photoacoustic images show a wall thickness of approximately 2 mm and near uniform contrast. The latter is a consequence of water being the dominant chromophore in each of the three layers of normal arterial tissue (intima,

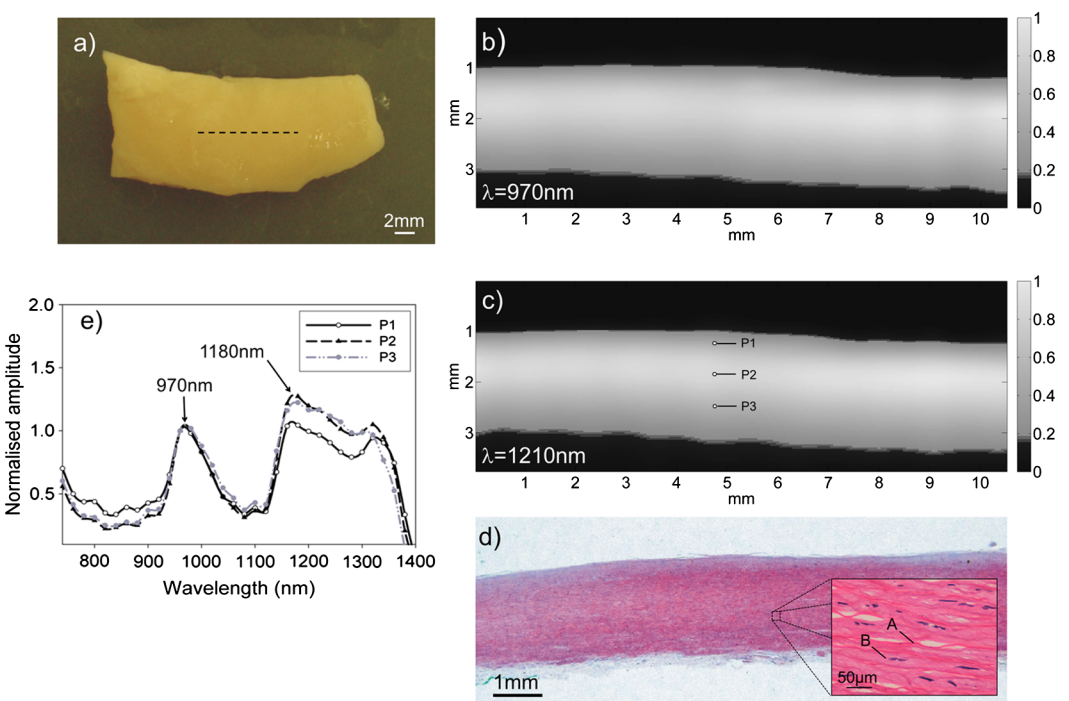

Fig. 4 (a) Photograph of a sample of normal human aorta. The horizontal dashed line represents the photoacoustic scan line. (b) Photoacoustic image obtained at 970 nm. The irradiated side is the top surface. (c) Photoacoustic image obtained at 1,210 nm. (d) Histological section; the inset shows a magnified (630×) photograph of the media (A: elastic fiber, B: smooth muscle cell). (e) Photoacoustic spectra obtained at three different points (P1, P2, and P3).

media, adventitia) at both 970 and 1210 nm. The histological section of the sample, which was obtained after the experiment, is shown in Fig. 4(d). This shows that the imaged cross-section is macroscopically relatively homogeneous, with no evidence of atheromatous plaque in agreement with the photoacoustic images. In addition, an inset shows a magnified (630×) photograph of a region, where finer structures such as elastic fibers and smooth muscle cells (SMCs) that are characteristic of the media in normal arterial tissue are evident.

Photoacoustic spectra (740 to 1400 nm) were obtained at three different spatial points, as indicated on Fig. 4(c). The spectra are shown in Fig. 4(e). For all three points, the spectra are broadly similar, with two main absorption peaks evident at 970 and 1180 nm. These peaks correspond to the absorption peaks of water, which is the dominant chromophore in arterial tissue at these wavelengths.

4.2 *Atheromatous Plaques*

To demonstrate the ability of the technique to characterize the structure and composition of atheromatous plaques, two different samples of human aortas displaying raised soft atherosclerotic lesions (as identified by visual inspection) were selected. 2-D cross-sectional images were then acquired at 970 and 1210 nm. Photoacoustic spectra in the 740 to 1400 nm spectral range were also obtained at selected points within the lesion and the normal surrounding tissue. The photoacoustic data were then compared to histological sections of the tissue.

4.2.1 *Sample 1*

A photograph of the sample is shown in Fig. 5(a), indicating the location of the lesion and the photoacoustic scan line. The tissue was scanned along this line over a length of 19 mm in steps of 500 μm. Figure 5(b) and 5(c) shows photoacoustic images of the tissue sample obtained at 970 and 1210 nm, respectively. The photoacoustic image obtained at 970 nm shows a relatively uniform contrast distribution, with the only indication of the presence of plaque being the thickening of the arterial wall. The arterial wall was 2 mm thick in the areas believed to be plaque free and 3 mm thick at the center of the lesion. The photoacoustic image obtained at 1210 nm shows a region of relatively strong contrast within the lesion. It is assumed this region is lipid-rich due to the high absorption coefficient of lipids at this wavelength [see Fig. 1(b)]. Since normal arterial tissue also absorbs at this wavelength, albeit to a lesser extent, the boundaries and interior of the sample remain visible. To remove the contribution of the absorbing constituents of the

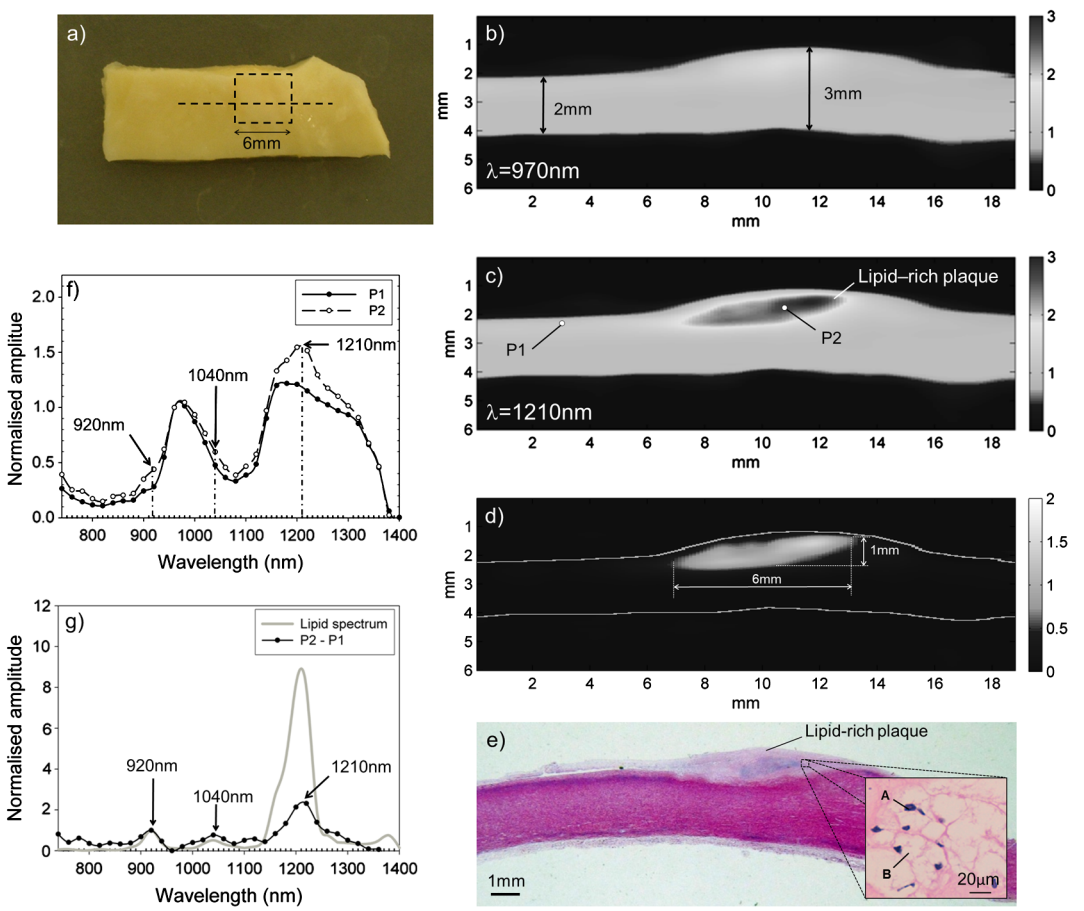

Fig. 5 (a) Photograph of a human aorta sample (sample 1) with a raised atherosclerotic lesion located within the dashed rectangle. The horizontal dashed line represents the photoacoustic scan line. (b) Photoacoustic image obtained at 970 nm. (c) Photoacoustic image obtained at 1,210 nm. (The darker region within the boundaries of the arterial wall represent high absorption.) (d) Image obtained by subtracting the two photoacoustic images in (b) and (c) to reveal the plaque region and overlaid with a segmented image of (c). (e) Histological section; the inset shows a magnified (630×) area of the lesion, confirming the presence of foamy macrophages. The nuclei of the foam cells are stained (H&E) blue (A). The cytoplasm of the cells is foamy and contains lipid droplets (B). (f) Photoacoustic spectra obtained at P1 and P2. (g) Photoacoustic spectrum obtained at P2 after subtracting the spectrum obtained in normal arterial tissue (P1). The spectrum of lipids is also shown for comparison.[35]

normal tissue and isolate the lipid-rich region, the images obtained at 1210 nm and at 970 nm were subtracted from each other, as shown in Fig. 5(d). This difference image is also overlaid with a segmented image of Fig. 5(b) to illustrate the location of the plaque within the boundaries of the arterial wall. The dimensions of the plaque were approximately 6 mm in length and 1 mm in thickness. Figure 5(e) shows a photograph of the histology section of the tissue sample. This confirms the presence of a lipid-rich plaque of similar shape and size. The inset shows a magnified image of a small region (110× 130 μm^2) of the lesion confirming the presence of lipid-engorged macrophages, called "foam cells," which are one of the main constituents of lipid plaques. These cells have their nucleus stained blue by the H&E and are characterized by the foaminess of their cytoplasm which contains small vacuoles of lipid droplets.

Photoacoustic spectra were obtained at two different spatial points at wavelengths between 740 to 1400 nm as indicated on Fig. 5(c). P1 corresponds to a region free of plaque, whereas P2 corresponds to a region within the plaque. Figure 5(f) shows the spectra obtained at both of these points. The spectrum obtained at P1 is similar to that shown in Fig. 4(e), where the broad absorption peaks of water at 970 and 1180 nm are dominant. These water absorption peaks are also visible in the spectrum obtained at P2; however, increases in absorption are also evident at 920, 1040, and 1210 nm, which correspond to the absorption peaks of lipids. These absorption peaks are not as distinctive as those in the lipid absorption spectrum in Fig. 1 because atherosclerotic plaques are complex lesions composed of a number of different constituents, such as lipids, macrophages, and calcium deposits as well as elastin, collagen, and water found in normal tissue.[1,2] Each of these constituents contributes to

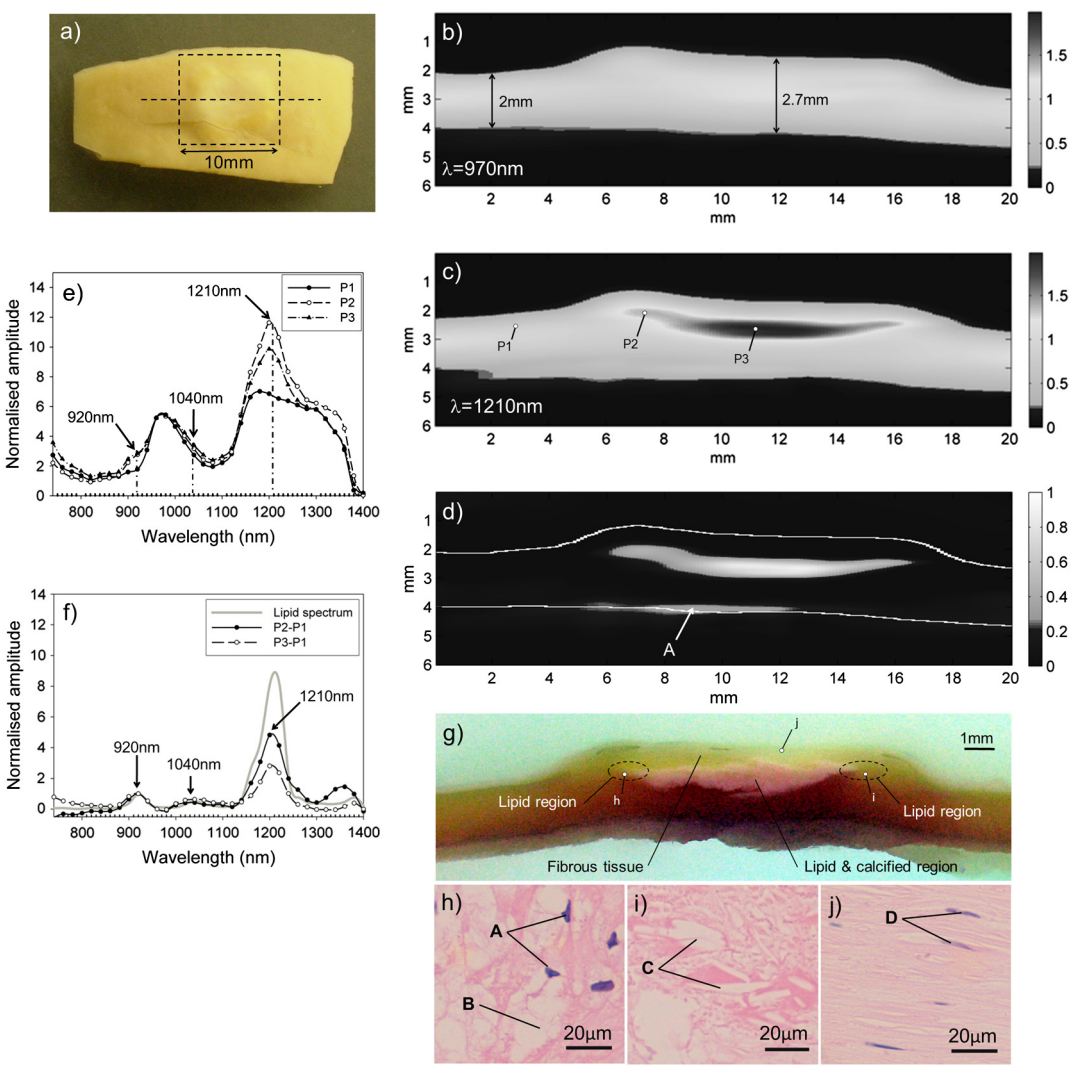

Fig. 6 (a) Photograph of a human aorta sample (sample 2) with a raised atherosclerotic lesion located within the dashed rectangle. The horizontal dashed line represents the photoacoustic scan line. (b) Photoacoustic image obtained at 970 nm. (c) Photoacoustic image obtained 1,210 nm. (The darker region within the boundaries of the arterial wall represent high absorption.) (d) Image obtained by subtracting the two photoacoustic images in (b) and (c) to reveal the plaque region and overlaid with a segmented image of (c). The arrow labeled A indicates an area of extravascular fat. (e) Photoacoustic spectra obtained at P1, P2, and P3. (f) Photoacoustic spectra obtained at P2 and P3 after subtracting the spectra obtained from normal arterial tissue (P1). The spectrum of lipids is also shown for comparison. (g) Photograph of the paraffin block prior to histological analysis. Photographs obtained from the histology slide of (h) foam cells (A: nucleus of the foam cells and B: lipids contained in the cytoplasm of a foam cell), (i) cholesterol clefts (C: clefts) and (j) fibrous tissue and smooth muscle cells (D: nucleus of smooth muscle cells). The location of these foam cells, cholesterol clefts, and fibrous tissue in (g) are labeled h, i, and j, respectively.

the photoacoustic spectra masking the absorption peaks of lipids. To observe the three absorption peaks of lipids more clearly, the spectral features attributed to normal arterial tissue were removed by normalizing the spectra obtained at P1 and P2 to the 970-nm water absorption peak and subtracting the spectrum obtained at P1 from that obtained at P2. The resulting difference spectrum is shown in Fig. 5(g) and is in broad agreement with the spectra of lipids, providing further configuration of lipid content.

These results show that the technique can image the full thickness of an atheromatous lesion with high contrast and spatial resolution and reveal the presence and morphology of a predominantly lipid-rich subsurface plaque.

4.2.2 *Sample 2*

The second tissue sample with a raised lesion was imaged along a length of 20 mm in steps of 500 μm. A photograph of the sample is shown in Fig. 6(a). Figure 6(b) and 6(c) shows 2-D photoacoustic images obtained at 970 and 1210 nm, respectively. The photoacoustic images obtained at 970 nm show relatively uniform contrast, and once again, the only indication of the presence of plaque is the thickening of the arterial wall. The wall thickness was measured from the photoacoustic image to be 2 mm in the region believed to be plaque free and 2.7 mm at the center of the lesion. The photoacoustic image obtained at 1210 nm shows an area of strong contrast suggesting the presence of lipids. Figure 6(d) shows the location of the lipid pool within the boundaries of the vessel. As described previously, this was obtained by subtracting the photoacoustic image obtained at 1210 nm from that obtained at 970 nm and overlaying with a segmented image of Fig. 6(c). In Fig. 6(d), a region of enhanced contrast was also present near the rear boundary of the arterial wall [labeled (A)], indicating the presence of a region of extravascular fat. Photoacoustic spectra were obtained from three different spatial points, as indicated on Fig. 6(c). P1 was taken from an area believed to be plaque-free, P2 and P3 were taken from areas believed to be lipid-rich. All three spectra are shown in Fig. 6(e). The spectrum obtained at P1 is very similar to that previously shown in Figs. 4(e) and 5(f) for plaque-free regions and dominated by the absorption peaks of water at 970 and 1180 nm. The spectra obtained at P2 and P3 display dominant absorption peaks at 970 and 1180 nm, which are also due to water absorption, as well as less prominent peaks at 920, 1040, and 1210 nm, which suggest the presence of lipids in these regions. Once again, the absorption peaks of lipids are more apparent in the spectra obtained at P2 and P3 [see Fig. 6(f)] after subtracting the normalized photoacoustic spectra obtained from a plaque-free region.

When the sample was initially being prepared for histological examination, it was found to contain significant calcification, which would need to be dissolved in order to section the tissue

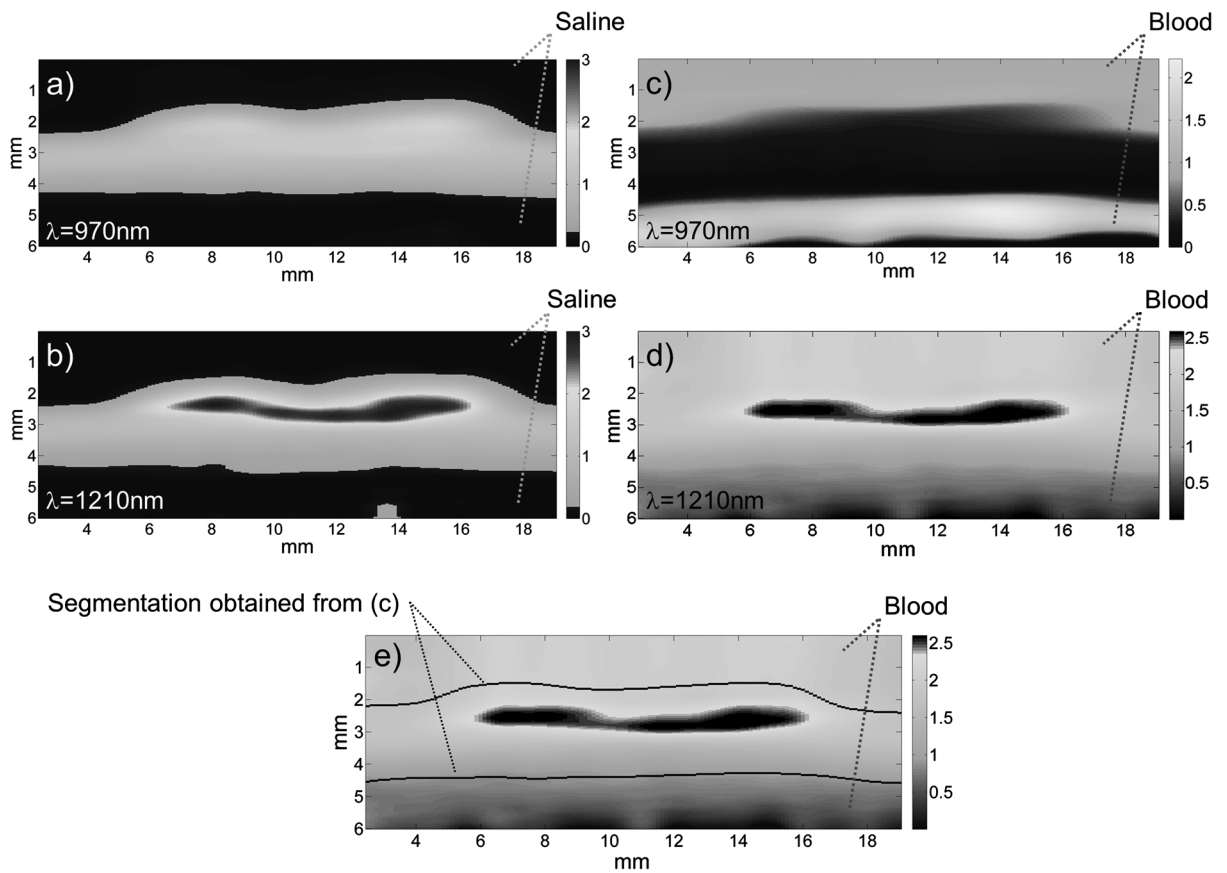

Fig. 7 Comparison of photoacoustic images of a human aorta sample (sample 2) with a raised lipid-rich plaque obtained when illuminating through saline and blood. Images obtained when illuminating the tissue sample through saline using an excitation wavelength of (a) 970 nm and (b) 1,210 nm. (The darker region within the boundaries of the arterial wall represent high absorption.) Photoacoustic images obtained through 2.8 mm of blood using an excitation wavelength of (c) 970 nm and (d) 1,210 nm. (e) Photoacoustic image obtained at 1,210 nm when imaging through blood, overlaid with a segmented image of (c).

sample. However, dissolving the calcium would result in the shape of the plaque being distorted when sectioned, to the extent that it could no longer be compared meaningfully to the photoacoustic images. For this reason, a two-step process was undertaken to determine the structure and composition of the sample. The first step involved progressively cutting back the paraffin block into which the tissue had been embedded for histological analysis until arriving at the location of the photoacoustic scan line. A photograph of the exposed cross-section of the tissue was then taken [see Fig. 6(g)]. The overall shape of the external boundaries and the thickness of the tissue in the photoacoustic images [Fig. 6(b)–6(d)] are in broad agreement with those in the photograph. The photograph also reveals a submerged plaque in approximately the same location as indicated in the photoacoustic images in Fig. 6(c) and 6(d). Two observations are made in relation to this feature. First, the submerged plaque is of a lighter hue than the surrounding tissue, which suggests the presence of calcium deposits. This in turn implies that there is also likely to be an abundance of lipids in this region since calcium deposits generally accumulate in lipid-rich areas (the photograph cannot reveal the presence of lipids directly)—an assertion that is consistent with the photoacoustic images and spectral data in Fig. 6, which indicate the presence of lipids in the same area. The second observation is that the horizontal dimension of the plaque in the photoacoustic images appears to be larger than the corresponding dimensions in the photograph. It is suggested that this is because the lateral extremities of the plaque contain little calcification and are dominated by an abundance of lipids, which are revealed by the photoacoustic images but not the photograph. To verify this, the second step in characterizing the tissue sample was undertaken. This involved preparing the sample for histological analysis by dissolving the calcified regions, sectioning it, and staining using hematoxylin and eosin (H&E). Figure 6(h) and 6(i) shows photographs of expanded regions of the histological section corresponding to the two areas marked "Lipid region" at the lateral extremities of the plaque in Fig. 6(g). These indicate the presence of foam cell nuclei, voids indicating the prior presence of lipids, and cholesterol clefts, all of which are hallmarks of lipid-rich plaque. Finally, Fig. 6(j) shows a photograph of the histological section corresponding to a region above the plaque. It reveals the presence of a fibrous matrix and smooth muscle cells with none of the abovementioned hallmarks of a lipid-rich plaque, suggesting that the cap of the lesion is a fibrous one. This is consistent with the photoacoustic image, which shows a region of uniform low contrast that indicates an absence of lipids above the high-contrast region corresponding to the lipid pool.

Overall, the following conclusions are drawn with respect to this sample. First, although under gross visual and tactile inspection, the lesion appeared to be a soft, predominantly lipid-rich plaque, histological analysis revealed it to be more complex, containing significant calcium as well as lipids. Second, although the photoacoustic images and spectral data allowed the plaque shape and dimensions to be accurately visualized, they were able to indicate the presence of only lipids, not calcification. This is because hydroxyapaitite, the main mineral found in calcification, does not have a sufficiently distinctive spectral signature in the 700 to 1400 nm wavelength range.[42,43]

4.3 *Imaging Through Blood*

As noted previously, if photoacoustic imaging is implemented in vivo using an intravascular fiber-optic probe, it would be desirable if the vessel wall could be imaged through several millimeters of blood (the order of the radius of the lumen of the coronary artery), rather than employing a saline flush. To investigate whether this is possible, the same human aorta sample as shown in Fig. 6(a) (sample 2) was imaged (over a different scan line) immersed initially in saline and then in blood. The thickness of blood between the tissue sample and the glass window that the excitation beam is incident on (Fig. 3) was 2.8 mm in the region of the normal arterial tissue. Figure 7(a) and 7(b) shows the photoacoustic images obtained in saline using excitation wavelengths of 970 and 1210 nm, respectively. Figure 7(c) and 7(d) shows the photoacoustic images obtained in blood using the same excitation wavelengths. The photoacoustic image obtained at 970 nm shows a stronger contrast from the blood-filled area surrounding the artery wall. This is due to the higher absorption coefficient of blood at this wavelength compared to that of arterial wall. However, the difference in the absorption coefficient of blood and normal arterial tissue still enables the boundaries of the arterial walls to be identified. The photoacoustic image obtained at 1210 nm showed a relatively strong contrast from the area believed to contain a plaque. The shape and dimensions of the plaque (10.4×0.9 mm^2) are in broad agreement with the photoacoustic image obtained when immersed in saline [Fig. 7(b)]. The boundaries of the arterial wall, however, could not be easily identified due to the blood surrounding the tissue sample providing similar contrast as to the arterial tissue at this wavelength. Figure 7(e) shows the photoacoustic image obtained at 1210 nm, when illuminated through blood, and overlaid with a segmented image of Fig. 7(c). These results show that by using these two wavelengths, it is possible to visualize the boundaries of the arterial wall and those of lipid-rich plaques when illuminating the sample through blood across physiologically relevant distances.

5 Discussion and Conclusions

This study has shown that photoacoustic imaging can visualize arterial tissue with high contrast and spatial resolution using excitation wavelengths in the 740 to 1400 nm spectral range. It has been demonstrated that it is possible to image the full thickness (~3 mm) of a raised atheromatous lesion on the wall of a human aorta with excellent signal to noise ratio (~30 dB). This suggests that it will be possible to visualize the entire wall thickness of even the most severely stenosed coronary artery. Furthermore, the feasibility of imaging through 2.8 mm of blood has also been demonstrated, suggesting that, unlike some other optical techniques, the use of a saline flush may not be required in an intravascular implementation. In this study, the vertical spatial resolution was limited by the detector bandwidth to 75 μm. By using a detector with a broader bandwidth, it should be possible to achieve a spatial resolution of 20 to 30 μm, limited ultimately by the frequency-dependent acoustic attenuation of tissue.

As well as providing high-resolution structural information, it has been shown that the presence of lipid-rich plaques can be ascertained using spectroscopic methods. By exploiting the strong preferential optical absorption of lipids at 1210 nm and imaging at multiple wavelengths, it has been shown that the location and boundaries of lipid-rich plaques can be visualized accurately in agreement with histological analyses. When imaging plaques containing both lipids and regions of calcification, the photoacoustic images obtained in this study were able to detect the presence of lipids, but not that of calcium deposits,

due to the spectrally indistinct nature of hydroxyapaitite in the 700 to 1400 nm wavelength range. The acoustic properties of calcium deposits, however, are significantly different from those of soft tissue, so one might expect them to produce reverberation-type distortions in the photoacoustic image, which could potentially be exploited to signify the presence of calcification. That it was not observed in this study may be because the relative concentration of hydroxyapaitite was insufficiently large. Further studies using a large number of samples with a greater variety of lesions types are required to explore this in more detail. If photoacoustic imaging is truly insensitive to this plaque component, then a multimodal approach combining photoacoustic imaging with pulse echo ultrasound or OCT may be required.

There are several future directions that may prove fruitful in terms of increasing the diagnostic sensitivity and specificity of the technique. In this study, a relatively unsophisticated *ad hoc* spectroscopic approach was employed: either a single excitation wavelength at the 1210 nm lipid absorption peak was employed to enhance selectively the contrast yielded by lipid-rich plaques or difference imaging was used to isolate the plaque boundary. While this simple approach serves to reveal the spatial distribution of the plaque, it does not provide a quantitative indication of its lipid content. However, using a model-based inversion spectroscopic inversion of the type previously used to quantify hemoglobin and other chromospheres,[44,45] it should be possible to provide images of the absolute concentration of lipids. As well as providing a quantitative measure of lipid content, which may be related to plaque vulnerability, this may help distinguish between plaques that are predominantly lipid-rich and those that are more complex (containing, for example, fibrous or calcified tissue as well as lipids). Although lipids represent the most obvious endogenous chromophore to target, other tissue constituents with more subtle spectral features, such as collagen and elastin, could potentially be identified and quantified using such spectroscopic methods, which are more sensitive than the simple method used in this study. This would also assist in providing more specific composition-related information for plaque characterization purposes. The strong optical absorption of blood at wavelengths below 1000 nm could also be exploited to visualize the structure and oxygen status of the vasa vasorum and detect intramural hemorrhages and explore their role in arterial disease. Through the use of spectrally distinct exogenous contrast agents there is further potential to detect other components such as macrophages[46–48] or specific biomolecules implicated in atherosclerosis.[49]

The challenge ahead in implementing the technique *in vivo* lies in achieving the necessary level of miniaturization for intravascular use. Several miniature photoacoustic probes based upon piezoelectric and optical ultrasound detectors of comparable dimensions to those required for intravascular imaging in human coronary arteries have now been developed and evaluated in tissue phantoms and ex vivo tissues.[28,50–52]

In summary, it is considered that intravascular spectroscopic photoacoustic imaging may find a role in the clinical detection, diagnosis, and treatment of arterial disease, either as a standalone technique or combination with existing intravascular imaging modalities.

Acknowledgments

The authors would like to thank Adrien Desjardins for his informative comments. This work was funded by the Engineering and Physical Sciences Research Council, UK. The authors would like to acknowledge Dr. Richard Caro of TangibleFuture Inc. for helpful early discussions relating to this work.

References

1. C. K. Glass and J. L. Witztum, "Atherosclerosis. The road ahead," *Cell* **104**(4), 503–516 (2001).
2. A. J. Lusis, "Atherosclerosis," *Nature* **407**(6801), 233–241 (2000).
3. F. D. Kolodgie et al., "The thin-cap fibroatheroma: a type of vulnerable plaque: the major precursor lesion to acute coronary syndromes," *Curr. Opin. Cardiol.* **16**(5), 285–292 (2001).
4. A. Tanaka, G. J. Tearney, and B. E. Bouma, "Challenges on the frontier of intracoronary imaging: atherosclerotic plaque macrophage measurement by optical coherence tomography," *J. Biomed. Opt.* **15**(1), 011104 (2010).
5. S. E. Nissen and P. Yock, "Intravascular ultrasound: novel pathophysiological insights and current clinical applications," *Circulation* **103**(1), 604–616 (2001).
6. G. J. Tearney, I.-K. Jang, and B. E. Bouma, "Optical coherence tomography for imaging the vulnerable plaque," *J. Biomed. Opt.* **11**(2), 021002 (2006).
7. H. Yabushita, "Characterization of human atherosclerosis by optical coherence tomography," *Circulation* **106**(13), 1640–1645 (2002).
8. S. H. Yun et al., "Comprehensive volumetric optical microscopy in vivo," *Nat. Med.* **12**(12), 1429–1433 (2006).
9. A. Maehara, G. S. Mintz, and N. J. Weissman, "Advances in intravascular imaging," *Circulation Cardiovasc. Interv.* **2**(5), 482–490 (2009).
10. I.-K. Jang et al., "Visualization of coronary atherosclerotic plaques in patients using optical coherence tomography: comparison with intravascular ultrasound," *J. Am. Coll. Cardiol.* **39**(4), 604–609 (2002).
11. Z. A. Fayad and V. Fuster, "Clinical imaging of the high-risk or vulnerable atherosclerotic plaque," *Circ. Res.* **89**(4), 305–316 (2001).
12. F. Sharif and R. T. Murphy, "Current status of vulnerable plaque detection," *Catheter. Cardiovasc. Interv.: Official Journal of the Society for Cardiac Angiography and Interventions* **75**(1), 135–144 (2010).
13. J. Sanz and Z. A. Fayad, "Imaging of atherosclerotic cardiovascular disease," *Nature* **451**(7181), 953–957 (2008).
14. K. C. Briley-Saebo et al., "Magnetic resonance imaging of vulnerable atherosclerotic plaques: current imaging strategies and molecular imaging probes," *J. Magn. Reson. Imaging* **26**(3), 460–479 (2007).
15. T. Saam et al., "The vulnerable, or high-risk, atherosclerotic plaque: noninvasive MR imaging for characterization and assessment," *Radiology* **244**(1), 64–77 (2007).
16. P. Beard, "Biomedical photoacoustic imaging," *Interface Focus* **1**(4), 602–631 (2011).
17. P. C. Beard and T. N. Mills, "Characterization of post mortem arterial tissue using time-resolved photoacoustic spectroscopy at 436, 461 and 532 nm," *Phys. Med. Biol.* **42**(1), 177–198 (1997).
18. S. Sethuraman et al., "Spectroscopic intravascular photoacoustic imaging to differentiate atherosclerotic plaques," *Opt. Express* **16**(5), 3362–3367 (2008).
19. J. D. Caplan et al., "Near-infrared spectroscopy for the detection of vulnerable coronary artery plaques," *J. Am. Coll. Cardiol.* **47**(8), C92–C96 (2006).
20. S. Waxman, "Near-infrared spectroscopy for plaque characterization," *J. Intervent. Cardiol.* **21**(6), 452–458 (2008).
21. P. R. Moreno, Detection of lipid pool, thin fibrous cap, and inflammatory cells in human aortic atherosclerotic plaques by near-infrared spectroscopy.," *Circulation* **105**(8), 923–927 (2002).
22. J. Wang et al., "Near-infrared spectroscopic characterization of human advanced atherosclerotic plaques," *J. Am. Coll. Cardiol.* **39**(8), 1305–1313 (2002).
23. T. J. Allen and P. C. Beard, "Photoacoustic characterisation of vascular tissue at NIR wavelengths," *Proc. SPIE* **7177**, 71770A1–71770A9 (2009).
24. T. J. Allen et al., "Photoacoustic imaging of lipid rich plaques in human aorta," *Proc. SPIE* **7564**, 75640C1 (2010).
25. B. Wang et al., "On the possibility to detect lipid in atherosclerotic plaques using intravascular photoacoustic imaging," *Conf. Proc.: Annual Intl. Conf. IEEE Eng. Med. Biol. Soc. 2009*, pp. 4767–4770, IEEE, Minneapolis (2009).

26. B. Wang et al., "Detection of lipid in atherosclerotic vessels using ultrasound-guided spectroscopic intravascular photoacoustic imaging," *Opt. Exp.* **18**(5), 4889–4897 (2010).
27. H.-W. Wang et al., "Label-free bond-selective imaging by listening to vibrationally excited molecules," *Phys. Rev. Lett.* **106**(23), 1–4 (2011).
28. K. Jansen et al., "Intravascular photoacoustic imaging of human coronary atherosclerosis," *Opt. Lett.* **36**(5), 597–599 (2011).
29. M. Keijzer et al., "Fluorescence spectroscopy of turbid media: Autofluorescence of the human aorta," *Appl. Opt.* **28**(20), 4286–4292 (1989).
30. M. J. van Gemert et al., "Optical properties of human blood vessel wall and plaque," *Lasers Surg. Med.* **5**(3), 235–237 (1985).
31. M. R. Prince et al., "Preferential light absorption in atheromas in vitro. Implications for laser angioplasty," *J. Clin. Invest.* **78**(1), 295–302 (1986).
32. R. L. P. van Veen et al., "Determination of visible near-IR absorption coefficients of mammalian fat using time- and spatially resolved diffuse reflectance and transmission spectroscopy," *J. Biomed. Opt.* **10**(5), 054004 (2011).
33. I. F. Cilesiz and A. J. Welch, "Light dosimetry: effects of dehydration and thermal damage on the optical properties of the human aorta," *Appl. Opt.* **32**(4), 477–487 (1993).
34. A. M. Nilsson et al., "Near infrared diffuse reflection and laser-induced fluorescence spectroscopy for myocardial tissue characterisation," *Spectrochimica acta. Part A, Mol. Biomol. Spectrosc.* **53A**(11), 1901–1912 (1997).
35. C. Tsai, J. Chen, and W. Wang, "Near-infrared absorption property of biological soft tissue constituents," *J. Med. Biol. Eng.* **21**(1), 7–13 (2001).
36. F. Duck, *Physical Properties of Tissue: A Comprehensive Reference Book*, Academic Press, Inc., San Diego (1990).
37. A. Orekhov et al., "Lipids in cells of atherosclerotic and uninvolved human aorta," *Exp. Mol. Pathol.* **42**(1), 117–137 (1985).
38. A. Roggan et al., "Optical properties of circulating human blood in the wavelength range 400-2500 nm.," *J. Biomed. Opt.* **4**(1), 36–46 (1999).
39. M. Cope, "The application of near infrared spectroscopy to non invasive monitoring of cerebral oxygenation in the newborn infant," PhD thesis University College London (1991).
40. H. F. Zhang et al., "Functional photoacoustic microscopy for high-resolution and noninvasive in vivo imaging," *Nat. Biotechnol.* **24**(7), 848–851 (2006).
41. Y. Saijo et al., "Acoustic properties of atherosclerosis of human aorta obtained with high-frequency ultrasound," *Ultra. Med. Biol.* **24**(7), 1061–1064 (1998).
42. T. M. Coelho et al., "Characterization of natural nanostructured hydroxyapatite obtained from the bones of Brazilian river fish," *J. Appl. Phys.* **100**(9), 094312 (2006).
43. E. A. Genina, A. N. Bashkatov, and V. V. Tuchin, "Optical clearing of cranial bone," *Adv. Opt. Technol.* **2008**, 1–8 (2008).
44. J. Laufer et al., "Quantitative spatially resolved measurement of tissue chromophore concentrations using photoacoustic spectroscopy: application to the measurement of blood oxygenation and haemoglobin concentration," *Phys. Med. Biol.* **52**(1), 141–168 (2007).
45. J. Laufer et al., "Quantitative determination of chromophore concentrations from 2D photoacoustic images using a nonlinear model-based inversion scheme," *Appl. Opt.* **49**(8), 1219–1233 (2010).
46. E. Yantsen et al., "Intravascular photoacoustic imaging with gold nanoparticles," *2007 IEEE Ultrasonics Symp. Proc.*, pp. 848–851, IEEE, New York, NY (2007).
47. B. Wang et al., "Plasmonic intravascular photoacoustic imaging for detection of macrophages in atherosclerotic plaques," *Nano Lett.* **9**(6), 2212–2217 (2009).
48. K. Douma, R. T. A. Megens, and M. A. M. J. van Zandvoort, "Optical molecular imaging of atherosclerosis using nanoparticles: shedding new light on the darkness," *Wiley Interdisciplinary Reviews. Nanomed. Nanobiotechnol.* **3**(4), 376–388 (2011).
49. D. Razansky et al., "Multispectral optoacoustic tomography of matrix metalloproteinase activity in vulnerable human carotid plaques," *Mol. Imaging Biol.* (2011) 10.1007/s11307-011-0502-6.
50. A. B. Karpiouk, B. Wang, and S. Y. Emelianov, "Development of a catheter for combined intravascular ultrasound and photoacoustic imaging," *Rev. Sci. Instrum.* **81**(1), 014901 (2010).
51. B.-Y. Hsieh et al., "Integrated intravascular ultrasound and photoacoustic imaging scan head," *Opt. Lett.* **35**(17), 2892–2894 (2010).
52. E. Z. Zhang and P. C. Beard, "A miniature all-optical photoacoustic imaging probe," *Proc. SPIE* **7899**, 78991F (2011).